JVI Journals.ASM.org

# The Influenza A Virus Protein NS1 Displays Structural Polymorphism

**Berenice Carrillo,[a] Jae-Mun Choi,[b] Zachary A. Bornholdt,[c] Banumathi Sankaran,[d] Andrew P. Rice,[a] B. V. Venkataram Prasad[a,b]**

Department of Molecular Virology and Microbiology, Baylor College of Medicine, Houston, Texas, USA[a]; Verna and Marrs McLean Department of Biochemistry and Molecular Biology, Baylor College of Medicine, Houston, Texas, USA[b]; Department of Immunology and Microbial Science, The Scripps Research Institute, La Jolla, California, USA[c]; Berkeley Center for Structural Biology, Lawrence Berkeley National Laboratory, Berkeley, California, USA[d]

**ABSTRACT**

**NS1 of influenza A virus is a potent antagonist of host antiviral interferon responses. This multifunctional protein with two distinctive domains, an RNA-binding domain (RBD) and an effector domain (ED) separated by a linker region (LR), is implicated in replication, pathogenesis, and host range. Although the structures of individual domains of NS1 from different strains of influenza viruses have been reported, the only structure of full-length NS1 available to date is from an H5N1 strain (A/Vietnam/1203/2004). By carrying out crystallographic analyses of full-length H6N6-NS1 (A/blue-winged teal/MN/993/1980) and an LR deletion mutant, combined with mutational analysis, we show here that these full-length NS1 structures provide an exquisite structural sampling of various conformational states of NS1 that based on the orientation of the ED with respect to RBD can be summarized as "open," "semi-open," and "closed" conformations. Our studies show that preference for these states is clearly dictated by determinants such as linker length, residue composition at position 71, and a mechanical hinge, providing a structural basis for strain-dependent functional variations in NS1. Because of the flexibility inherent in the LR, any particular NS1 could sample the conformational space around these states to engage ED in different quaternary interactions so that it may participate in specific protein-protein or protein-RNA interactions to allow for the known multifunctionality of NS1. We propose that such conformational plasticity provides a mechanism for autoregulating NS1 functions, depending on its temporal distribution, post-translational modifications, and nuclear or cellular localization, during the course of virus infection.**

**IMPORTANCE**

**NS1 of influenza A virus is a multifunctional protein associated with numerous strain-specific regulatory functions during viral infection, including conferring resistance to antiviral interferon induction, replication, pathogenesis, virulence, and host range. NS1 has two domains, an RNA-binding domain and an effector domain separated by a linker. To date, the only full-length NS1 structure available is that from an H5N1 strain (A/Vietnam/1203/2004). Here, we determined crystal structures of the wild type and a linker region mutant of the H6N6 NS1 (A/blue-winged teal/MN/993/1980), which together with the previously determined H5N1 NS1 structure show that NS1 exhibits significant strain-dependent structural polymorphism due to variations in linker length, residue composition at position 71, and a mechanical hinge. Such a structural polymorphism may be the basis for strain-specific functions associated with NS1.**

Influenza A virus, a member of the *Orthomyxoviridae* family, is the causative agent of seasonal flu epidemics, and the highly pathogenic H5N1 avian strains currently pose a threat for a worldwide pandemic. The increased lethality observed in the H5N1 strains has been partly attributed to the NS1 protein (1–3), which all influenza viruses use to counter the host immune response (4–6). NS1 is important for several viral functions, including suppressing apoptosis through interactions with the p85β regulatory subunit of phosphoinositide 3-kinase (PI3K), regulating mRNA processing via interactions with the cleavage and polyadenylation and specificity factor 30 (CPSF30), limiting the activity of protein kinase R (PKR) (7), and inhibiting the induction of the 2′5′ oligonucleotide A synthetase (OAS)/RNase L pathway by binding to double-stranded RNA (dsRNA) (8). This multifunctional protein is composed of two domains, an RNA-binding domain (RBD) and an effector domain (ED), which are connected by a short linker region (LR).

Although several crystal structures of the individual domains of NS1 (9–12), as well as complexes of ED with various binding partners, have been determined (9, 13, 14), details pertaining to their specific protein-protein interactions in the context of a full-length (FL) NS1 remain unclear. Understanding the complex interactions of FL NS1 has become important, since many of the functions of NS1 are strain specific (13, 15–18) and have been associated with sequence variations that occur among strains, such as naturally occurring truncations at the C terminus (19, 20) and deletions at the linker region (20, 21). NS1 typically has an LR length of 12 residues. Interestingly, most NS1 proteins from highly pathogenic avian influenza viruses of the H5N1 subtype have a 5-amino-acid (aa) deletion (residues 80 to 84) in the LR that has been maintained since 2000 and has been shown to contribute to virulence (1, 20, 22), suggesting that this 5-aa deletion confers a replicative advantage. Currently, the only FL crystal structure available of NS1 is that of an H5N1 strain (A/Vietnam/1203/2004; referred to here as VN/04 H5N1-NS1), which is representative of only a minority of NS1 proteins among influenza viruses since it contains the 5-aa deletion in the LR (23). The

**Received** 13 December 2013 **Accepted** 17 January 2014
**Published ahead of print** 29 January 2014
**Editor:** W. I. Sundquist
Address correspondence to B. V. Venkataram Prasad, vprasad@bcm.edu.

doi:10.1128/JVI.03692-13

VN/04 H5N1-NS1 crystal structure showed that NS1 forms a dimer via the RBD, with the two ED domains flanking the RBD dimer. In addition, within the crystal lattice of the VN/04 H5N1-NS1, NS1 forms higher-order oligomeric structures through ED-ED interactions with neighboring NS1 molecules. Thus far, the structure of the FL NS1 without a 5-aa deletion that would be representative of the majority of NS1s has not been determined. Therefore, the effect that a longer LR would have on the relative orientation of two domains and consequently on the quaternary interactions, which may profoundly influence the ability of NS1 to interact with various host proteins, has remained unexplored.

To examine how the length of the LR affects the relative orientations of the ED and RBD, whether it affects the domain structures, and whether the two domains engage in similar quaternary interactions as observed in the VN/04 H5N1-NS1 structure, we determined the crystal structure of an H6N6 strain (A/blue-winged teal/MN/993/1980) (referred to here as H6N6-NS1) that has an LR typically observed in the majority of NS1s. To further examine whether the structural characteristics of the VN/04 H5N1-NS1 can be mimicked, we determined the crystal structure of the H6N6-NS1Δ80-84 mutant. These structural analyses revealed that the length of the linker, the residue composition at position 71, and a mechanical hinge have a profound influence on the relative orientation between the two domains. Our structures of two full-length NS1s, along with the previously published structure of the VN/04 H5N1-NS1 and in combination with mutational analysis, show that these FL-NS1 structures provide a structural sampling of strain-dependent conformational states that, based on the orientation of the ED with respect to RBD, can be summarized as "open," "semi-open," and "closed" conformations. These structures also show that irrespective of the LR length, NS1 is able to self-associate into higher-order oligomers through various ED-ED interactions, including the conserved type A ED-ED interactions that are important for FL-NS1 binding to dsRNA. These results help in understanding the strain-dependent functions of NS1, which may be a result of the altered structural flexibility that may exist among NS1s due to sequence variations particularly in the regions close to the LR.

## MATERIALS AND METHODS

**Plasmid construction.** The FL H6N6-NS1 (A/blue-winged teal/MN/993/1980) coding sequence was cloned into pET-46-Ek/LIC (Novagen) with an N-terminal thrombin site to remove the His tag. Site-directed mutagenesis using a QuikChange mutagenesis kit (Agilent Biotechnologies) was used to introduce R38A and K41A mutations to prevent precipitation as described previously (23). The sequences for the point mutations were as follows: forward primer, 5′-CTTGACCG GCTTCGCGCAGATCAGGCGTCTCTAAGAGGAAG-3′, and reverse primer, 5′-CTTCCTCTTAGAGACGCCTGATCTGCGCGAAGCCGGT CAAG-3′. The pET46-FL-H6N6-NS1 R38A/K41A plasmid was then used to generate pET46-H6N6-NS1Δ80-84. Site-directed mutagenesis using a QuikChange mutagenesis kit was performed to delete 15 residues (aa 80 to 84). The sequences for the deletional mutagenesis are as follows: forward primer, 5′-ACGAGGCACTCAAAATGCCTGCCTCACGCTAC-3′, and reverse primer, 5′-GTAGCGTGAGGCAGGCATTTTGAGTGCCTCGT-3′.

pET46-FL-H6N6-NS1 R38A/K41A and pET46-VN/04 H5N1-NS1 R38A/K41A were used to generate the W187Y mutations on each individual plasmid. Site-directed mutagenesis using a QuikChange mutagenesis kit was performed to make the W187Y mutation. Since the region encompassing this residue is conserved in both H6N6-NS1 and VN/04 H5N1-N1, we utilized the same primers to make the W187Y mutations. The primers used to generate these constructs were as follows: forward primer, 5′-GTCCTCATCGGAGGACTTGAATACAATGATAACACAGTTCGAG -3′, and reverse primer, 5′-CTCGAACTGTGTTATCATTGTATTCAAG TCCTCCGATGAGGAC-3′.

pET46-FL-H6N6-NS1 R38A/K41A/W187Y and pET46-VN/04 H5N1-NS1 R38A/K41A/W187Y were used to PCR amplify H6N6-NS1-ED and VN/04 H5N1-NS1-ED inserts, respectively. The primers used to PCR amplify H6N6-NS1-ED to generate pET46-H6N6-NS1-ED W187Y were as follows: forward primer, 5′-GACGACGACAAGATGTTAGTGCCACGA GGAAGC-3′, and reverse primer, 5′-TCAAACTTCTGACTCAATTGTT CTCGCC-3′. The primers used to PCR amplify VN/04 H5N1-NS1 W187Y ED and to generate pET46-H5N1-NS1-ED W187Y were as follows: forward primer, 5′-TTAGTGCCACGAGGAAGCATGCCGG-3′, and reverse primer, 5′-TTACCGTTTCTGATTTGGAGGGAGTGGAAG-3′.

**Protein expression and purification.** The pET-46-H6N6-NS1 R38A/K41A construct was expressed in *Escherichia coli* BL21(DE3) cells at 37°C to an $A_{600}$ of 0.8, induced with 0.5 mM IPTG (isopropyl-β-D-thiogalactopyranoside), and allowed to express overnight at 25°C. Bacterial pellets were resuspended with 25 ml of lysis buffer (50 mM $NaH_2PO_4$, 300 mM NaCl, 10 mM imidazole [pH 8.0]) and lysed using a microfluidizer. NS1 was purified from clarified lysate using standard nickel-affinity purification with Ni-nitrilotriacetic acid (NTA) agarose beads (Qiagen). The beads were washed three times with wash buffer (50 mM $NaH_2PO_4$, 300 mM NaCl, 30 mM imidazole [pH 8.0]) and then washed three times in 50 ml of 10 mM HEPES–200 mM NaCl (pH 8.0) buffer. The bead-protein slurry was then resuspended in 25 ml of 10 mM HEPES–200 mM NaCl (pH 8.0) buffer and treated with thrombin overnight at 4°C to cleave H6N6-NS1 from the beads. The protein was then passed through size-exclusion chromatography to remove thrombin. Purified H6N6-NS1 was concentrated to 11 mg/ml in 10 mM HEPES–200 mM NaCl (pH 8.0) buffer.

The pET46-H6N6-NS1Δ80-84 construct was expressed in *E. coli* BL21(DE3) cells at 37°C to an $A_{600}$ of 0.9, induced with 1 ml of 1 M IPTG, and subjected to induction to continue for 4 h. Bacterial pellets were resuspended with 25 ml of lysis buffer and lysed using a microfluidizer. H6N6-NS1Δ80-84 was purified from clarified lysate using standard nickel-affinity purification with Ni-NTA agarose beads (Qiagen). The beads were washed three times with wash buffer (50 mM $NaH_2PO_4$, 300 mM NaCl, 30 mM imidazole [pH 8.0]) and then resuspended in 25 ml of wash buffer before being treated with thrombin for 5 h at room temperature to cleave H6N6-NS1Δ80-84 from the beads. The protein was then dialyzed into 10 mM HEPES–200 mM NaCl (pH 8.0) buffer and subjected to size exclusion chromatography to remove thrombin. Purified H6N6-NS1Δ80-84 was concentrated to 9 mg/ml in 10 mM HEPES–200 mM NaCl (pH 8.0) buffer.

The pET46-H6N6-NS1-ED W187Y and pET46-H5N1-NS1-ED W187Y mutants were expressed by following the same purification protocol as that for the full-length pET-46-H6N6-NS1 R38A, K41A construct. The choice for the W187Y mutation was made since such a mutation would be less drastic and less likely to affect the local structure and also based on previous studies (16) suggesting that this particular mutation only affected ED-ED interactions but not the ED interactions with CPSF30. Both ED W187Y mutant proteins were dialyzed into 10 mM HEPES–200 mM NaCl (pH 8.0) buffer.

**Crystallization and data collection.** Purified FL H6N6-NS1 was used for crystallization by the hanging-drop method. Crystals were obtained by mixing 1:1 ratios of FL H6N6-NS1 protein (11 mg/ml) and well solution containing 400 mM magnesium formate and 15% methanol. Crystals were grown at 22°C and formed in a month. Crystals were harvested and cryoprotected by shock soaking in 400 mM magnesium formate, 15% methanol, and 23% glycerol. Purified H6N6-NS1Δ80-84 was used for crystallization by the hanging-drop method. Crystallization of H6N6-NS1Δ80-84 was achieved by mixing 1:1 ratios of H6N6-NS1Δ80-84 protein (9 mg/ml) and well solution containing 200 mM KSCN, 20% PEG 3350, and 100 mM HEPES (pH 7.0). A 10 mM stock of L-glutathione reduced (GSH)/L-glutathione oxidized (GSSG) (Hampton Additive

**TABLE 1** Data collection, phasing, and refinement statistics[a]

| Parameter | H6N6-NS1 | H6N6-NS1Δ80-84 |
|---|---|---|
| Data collection statistics | | |
| Space group | $P6_122$ | $P2_1$ |
| Unit cell dimensions | | |
| *a*, *b*, *c* (Å) | 101.69, 101.69, 119.53 | 43.87, 120.85, 53.26 |
| α, β, γ (°) | 90.00, 90.00, 120.00 | 90.00, 103.42, 90.00 |
| Wavelength (Å) | 1.0000 | 0.9774 |
| Resolution range (Å) | 88.04–3.16 (3.33∼3.16) | 60.44–2.70 (2.74∼2.70) |
| $R_{merge}$ (%) | 0.136 (0.933) | 0.074 (0.906) |
| $R_{Pim}$ (%) | 0.042 (0.281) | 0.051 (0.630) |
| Avg $I/\sigma$ | 12.6 (2.4) | 7.5 (1.0) |
| Completeness (%) | 100 (100) | 94.8 (97.0) |
| Multiplicity | 11.1 (11.7) | 2.8 (2.8) |
| Refinement statistics | | |
| Resolution range (Å) | 88.04–3.16 | 60.44–2.7 |
| No. of reflections | 6,704 | 14,455 |
| $R_{work}/R_{free}$ | 0.2302/0.2864 | 0.2151/0.2635 |
| No. of atoms | | |
| Protein | 1,527 | 2,943 |
| Ligand/ion | 0 | 0 |
| Water | 0 | 0 |
| B factors (Å$^2$) | | |
| Protein | 60.10 | 74.74 |
| Ligand/ion | NA | NA |
| Water | NA | NA |
| RMSD | | |
| Bond length (Å) | 0.0103 | 0.007 |
| Bond angle (°) | 1.522 | 0.975 |

[a] The highest-resolution shell values are shown shown in parenthesis. NA, not applicable.

Screen) was used as an additive. Crystals were grown at 22°C and formed after a week. Crystals were harvested and cryoprotected by shock soaking in 200 mM KSCN, 20% PEG 3350, 100 mM HEPES, and 28% glycerol (pH 7.0). Data for H6N6-NS1 and H6N6-NS1Δ80-84 were collected at Advanced Light Source using beamline 5.0.1.

**Data processing and structure determination.** Crystals of FL H6N6-NS1, belonging to the $P6_122$ space group, and H6N6-NS1Δ80-84, belonging to the $P2_1$ space group, diffracted to resolutions of 3.1 and 2.7 Å, respectively. Diffraction data for both crystals were processed using iMosflm (24) and scaled using SCALA, as implemented in the CCP4 6.0.2 software package (25). The Quicksym subprogram in iMosflm unequivocally identified the space groups. Since the diffraction data for FL H6N6-NS1 were anisotropic, the data were corrected for anisotropy using the UCLA MBI server (26), which suggested truncation of data to ∼3.16 Å. The resulting data were used for molecular replacement (MR) and refined with the PHENIX package (27) (Table 1). For monitoring the refinement, 5% of the data were set aside for $R_{free}$ calculations (28). The PR8 H1N1 ED (Protein Data Bank [PDB] ID 2GX9) and RBD of H5N1 NS1 (PDB ID 3F5T) were separately used as search models for MR using the program PHASER. After MR, iterative cycles of model building using COOT (29), density modification (30), and phenix.refine (27) were carried out. During the course of the refinement, the stereochemistry of the structures was checked using Molprobity (31). The statistics of data collection and final refinement are shown in Table 1. Structural figures were made using PyMOL (The PyMOL Molecular Graphics System, v1.5.0.4 [Schrödinger, LLC]). The buried surface area calculation and interface analysis were performed using the PISA server (http://www.ebi.ac.uk/msd-srv/prot_int/pistart.html).

**RCSB accession codes.** The coordinates and structure factors for the two crystal structures determined in the present study have been deposited in the PDB under the accession codes 4OPH (FL H6N6-NS1) and 4OPA (H6N6-NS1Δ80-84).

## RESULTS

**Subunit structure of FL H6N6-NS1 shows unsuspected interdomain interactions.** The FL H6N6-NS1, expressed and purified following the protocol for the VN/04 H5N1-NS1 (23), crystallized in the $P6_122$ space group and contains one molecule in the asymmetric unit (AU). The structure was determined by using molecular replacement to a resolution of 3.16 Å (Table 1). The overall polypeptide folds of the RBD and the ED in the H6N6 NS1 are similar to previously determined structures of the individual domains (10, 12, 23) (Fig. 1A). The LR connecting the RBD and ED, with a clear electron density (Fig. 1A), shows an extended random coil structure except for a well-defined type I β-turn from residues 74 to 77 (Fig. 1A inset I). This β-turn allows for a change in the direction of the polypeptide chain, permitting the ED to fold back and be in close proximity to the RBD and creating a relatively compact structure. Such a disposition of the two domains allows for interdomain hydrogen bond interactions involving side chains of Arg59 and Gln63 of the RBD and Gly168 and Thr170 (170-loop) of the ED, which further stabilize the compact structure (Fig. 1A, inset II).

Upon inspection of the crystal packing of H6N6 NS1, we observed that pairs of NS1 molecules, related by crystallographic 2-fold axis, intertwine through their LRs, with each ED subunit positioned at an angle with respect to RBD dimer to form a Y-shaped dimer (Fig. 1B). Approximately 1,882 Å$^2$ of total surface area is buried in the formation of this NS1 "dimer" mainly involving the RBD. Moreover, Ile81 LR residues of the opposing subunits in the dimer are involved in backbone hydrogen bonding interactions. The observation that the NS1 dimers are "intertwined" in pairs and that the LR is not involved in any crystal contacts suggests that NS1 dimerization takes place prior to any subsequent formation of higher-order oligomeric structures.

**Linker length dramatically alters the angular disposition between the domains.** To examine the effect of LR length on the angular disposition of the RBD and ED, we superimposed H6N6-NS1 and VN/04 H5N1-NS1 subunits with respect to their RBDs. Superposition clearly shows how the linker length dramatically alters the relative orientation between RBD and ED (Fig. 1C). Except for the difference in the angular disposition of the two domains in the two NS1 structures, the overall structures of the RBD and ED in both structures are well conserved with the root mean square deviations (RMSDs) of 0.848 and 0.5 Å, respectively. Comparison of these two structures shows that the interdomain interactions that were observed in the H6N6-NS1 subunit structure are absent in the VN/04 H5N1-NS1 structure, despite the conservation of the participating residues.

**The H6N6-NS1 forms two types of chain-like structures via ED-ED interactions.** The formation of higher-order oligomeric structures by NS1, particularly tubular structures, has been shown to be important for binding dsRNA to prevent the induction of the 2′5′(OAS)/RNase L pathway (23, 32). To examine whether H6N6-NS1 formed higher-order oligomeric structures that resemble chains, as observed in the VN/04 H5N1-NS1 crystal structure, we analyzed intermolecular interactions in the crystal lattice of the H6N6-NS1 structure. Although there is only one type of RBD-RBD interaction, two distinct types of ED-ED interactions can be visualized in the crystal lattice of H6N6-NS1. Each ED, in

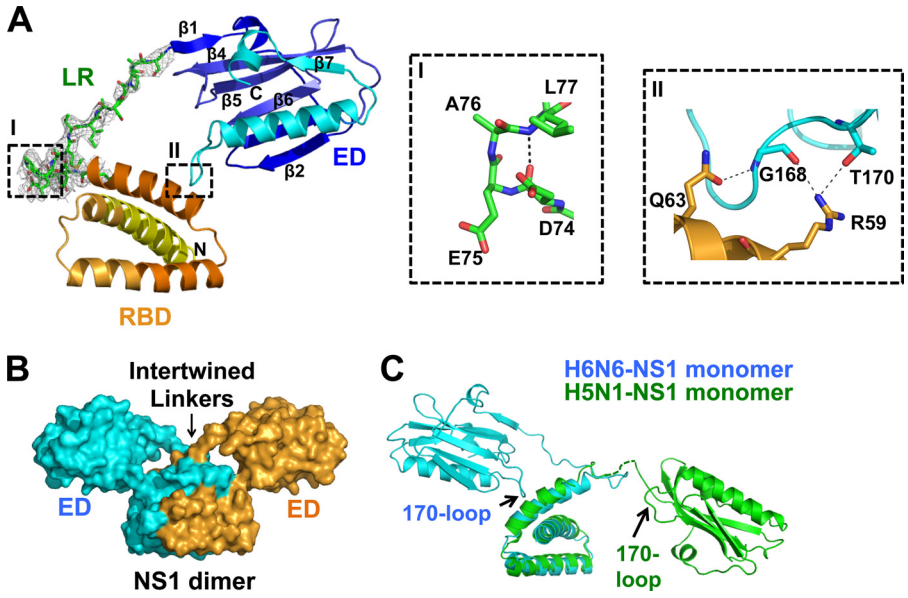


**FIG 1** H6N6-NS1 structure. (A) Diagram representation of H6N6-NS1 structure with the RNA-binding domain (RBD) (yellow to orange), linker region (LR) (green), and effector domain (ED) (blue to cyan). The N and C termini of NS1 are denoted as N and C, respectively. β-Strands are numbered in the ED. The simulated annealing omit difference map contoured at ~3σ for residues 71 to 84 in the H6N6-NS1 structure is shown as a gray mesh. Inset I shows a type I β-turn in the LR. Inset II shows intramolecular interactions between the RBD (orange) and the 170-loop of the ED (cyan). Residues involved in hydrogen bonding are shown as sticks, and hydrogen bonds are shown as dashed gray lines. (B) The NS1 dimer, with one subunit in cyan and the other in bright orange, is mediated by the RBD-RBD dimeric interactions, with the EDs positioned above the RBDs at an angle conferring the dimer a Y shape. An arrow indicates the area in which the LRs of each NS1 subunit in the dimer become intertwined. (C) Superposition of the H6N6-NS1 (cyan) and the VN/04 H5N1-NS1 (green) (PDB ID 3F5T) structures showing significant differences in their ED orientations with respect to RBD. Disordered residues (75 to 79) in the LR of VN/04 H5N1-NS1 (PDB ID 3F5T) structure are shown as a dotted green line.

the dimer described above, makes contacts with two other EDs from neighboring NS1 molecules. The first type of ED-ED interaction, with a buried surface area of 535 Å$^2$, is mostly mediated by a long α-helix (aa 171 to 188) in each ED (Fig. 2A). Such ED-ED interactions have been previously observed in the crystal structures of the ED alone (15) and in the VN/04 H5N1-NS1structure (23) (here referred to as type A ED-ED interactions). The second type of ED-ED interaction that is observed in the H6N6-NS1

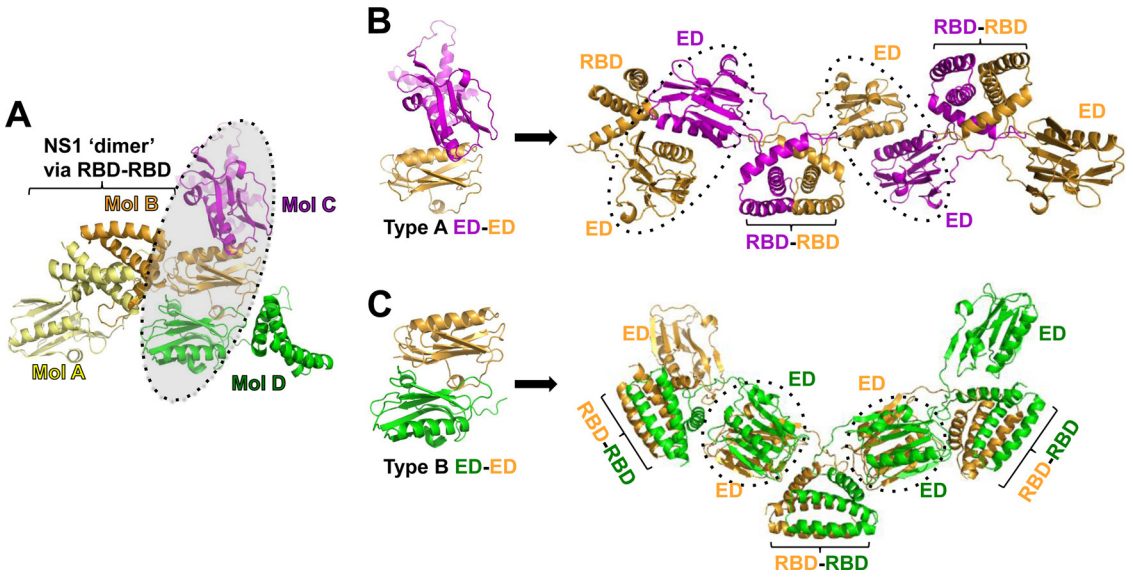


**FIG 2** Higher-order interactions formed by crystal packing of H6N6-NS1. (A) The NS1, forming a "dimer" via RBD-RBD interactions, is shown in light yellow for molecule A (Mol A) and bright orange for molecule B (Mol B). Each ED in the NS1 "dimer" is involved in two types of ED-ED interactions (dashed circle) in the crystal (each depicted with respect to the ED of Mol B for clarity) with neighboring NS1 molecules: molecule C (Mol C) in magenta and molecule D (Mol D) in green. (B) The type A ED-ED interaction between the ED of Mol C (magenta) and the ED of Mol B (bright orange) is mediated by the long α-helix of each ED, which links the "dimers" of NS1 into zigzag chains (each NS1 is interchangeably colored magenta and bright orange). (C) The type B ED-ED interactions between the ED of Mol B (bright orange) and the ED of Mol D (green) links NS1 "dimers" into helical chains (each NS1 is interchangeably colored green and bright orange). In panels A and B, the dotted circles highlight the linkages of the NS1 "dimers" into chains created by type A and B ED-ED interactions, respectively.

structure, which is related by a crystallographic 2-fold axis, involves β-strand 1 (Fig. 1A) and the loop region following β-strand 2 (Fig. 1A) and has a buried surface area of 765 Å$^2$ (referred to here as type B ED-ED interactions) (Fig. 2B). Such an ED-ED interaction was not observed in the VN/04 H5N1-NS1. Instead of the type B interactions, the VN/04 H5N1-NS1 exhibits a different type of ED-ED interaction involving β-strand 1, N-terminal α-helix, β-strand 4, β-strand 7, and a C-terminal α-helix. Depending on the type of ED-ED interaction that is followed in the H6N6-NS1 crystal, two types of NS1 chains can be visualized: a zigzag chain involving type A ED-ED interaction (Fig. 2A) and a helical chain involving type B ED-ED interactions (Fig. 2B). These observations show that the ED of the H6N6-NS1, like that of VN/04 H5N1-NS1, engages in the formation of higher-order oligomers. In particular, type A ED-ED interactions, important to binding dsRNA, are conserved in both crystal structures. However, the nature of the quaternary interactions varies because of the LR length.

**Type A ED-ED interaction is not obligatory for forming higher-order oligomers in solution.** Although various types of ED-ED interactions have been observed (12), only type A ED-ED interactions, which involve the insertion of Trp187 into the hydrophobic pocket of a neighboring ED, have been shown to be important for the cooperative binding of NS1 to dsRNA (16, 32–34). Because we observed two types of ED-ED interactions in our H6N6-NS1 crystal structure, we wanted to determine whether H6N6-NS1 exhibited a distinct preference for type A ED-ED interactions in solution. We mutated Trp187 to tyrosine in the H6N6-NS1 and analyzed its ability to form dimers and multimers in solution. The gel filtration profile of the H6N6-NS1 W187Y mutant showed a major peak corresponding to a dimer, as well as a broad peak corresponding to higher-molecular weight-oligomers (Fig. 3A). Similar results were obtained with a VN/04 H5N1-NS1 W187Y mutant in which the major peak corresponds to the NS1 dimer and also forms multimers, albeit to a lesser extent than the H6N6-NS1 wild type and the W187Y mutant (Fig. 3A). In addition, we also analyzed the oligomeric state of H6N6-NS1 using analytical gel filtration at concentrations ranging from 11 to 92 μM and found that the H6N6-NS1 remained dimeric at these concentrations (data not shown). To ensure that the W187Y mutation did indeed disrupt the type A ED-ED interaction, we made ED constructs of both, H6N6-NS1 and VN/04 H5N1-NS1 containing the W187Y mutation. The gel filtration profiles showed type A ED-ED interactions were disrupted as the ED constructs of both strains eluted as monomers (Fig. 3B). Taken together, our studies show that FL-NS1 can form dimers and higher-order oligomers, even in the absence of type A ED-ED interactions. This is consistent with a previous model suggesting that while the RBD provides the main dimeric interface, it can be transient (15). It is possible that NS1 utilizes its ability to form higher-order oligomeric structures through different types of ED-ED interactions depending upon its functional context during the infection process.

**The 5-aa deletion in the LR of H6N6-NS1 results in the formation of a novel closed dimer.** To examine whether shortening the LR of the H6N6-NS1 would recapitulate the interdomain orientation that was observed in the crystal structure of VN/04 H5N1-NS1, we made a H6N6-NS1 construct in which LR residues 80 to 84 were deleted (denoted as H6N6-NS1Δ80-84), thus mimicking the shortened linker of the VN/04 H5N1-NS1. The crystal structure of this construct, in the $P2_1$ space group, was determined

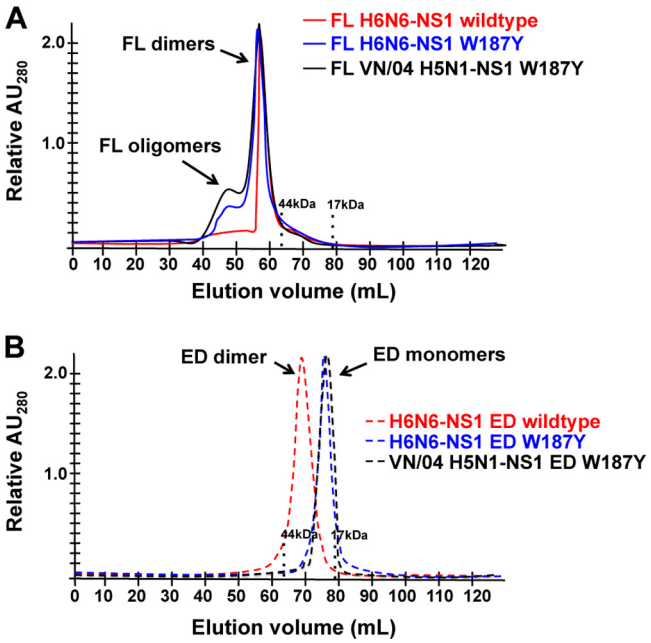


**FIG 3** Size-exclusion chromatography of wild-type and W187Y mutants of NS1. (A) The gel filtration profile (Superdex S75) for the wild-type FL H6N6-NS1 (solid red line) shows formation of dimeric and higher-molecular-weight structures which coincide with the gel filtration profiles of its W187Y mutant (solid blue line) and also that of VN/04 H5N1-NS1 W187Y mutant (solid black line). (B) The gel filtration profile for the wild-type H6N6 ED construct (dashed red line) shows a dimer. In contrast, the W187Y mutant of the H6N6-NS1 ED construct (dashed blue line) shows a monomeric ED. The VN/04 H5N1-NS1 ED construct with W187Y mutation (solid black line) also runs as a monomer. Thus, W187Y mutation disrupts type A ED-ED contacts in the NS1 of both H6N6 and H5N1 in the context of ED alone. Standards for 44- and 17-kDa proteins are shown as vertical dashed lines.

to 2.7 Å using molecular replacement techniques (Table 1). Surprisingly, in this crystal structure, the two molecules in the AU interact with each other forming a closed dimer involving both ED and RBD interactions between the opposing subunits. This finding is in contrast to dimers observed in either wild-type H6N6-NS1 or the VN/04 H5N1-NS1 structures in which only the RBD is involved in dimer formation (Fig. 4B). The EDs in the H6N6-NS1Δ80-84 dimer, instead of flanking the RBD dimer as in the VN/04 H5N1-NS1 crystal structure, are placed right above the RBD dimer. With the involvement of both the domains, the dimer interface in H6N6-NS1Δ80-84 is extensive, with a total buried surface area of 2,152 Å$^2$. In this closed dimer, while the RBD-RBD interactions are totally maintained, the ED-ED interactions are novel, involving contacts between Ser82 (after renumbering following 5-aa deletion, as in VN/04 H5N1-NS1 sequences) of one subunit and Tyr84 of the opposing subunit in the dimer.

Structural alignment of the two NS1 subunits in the AU that form the dimer in the H6N6-NS1Δ80-84 structure revealed that they display slightly different interdomain orientations (Fig. 4C). To identify which region in the LR could impart this flexibility, we carried out domain motion analysis of these two conformations using DynDom software (35), which suggested that residues Met79 and Pro80 (after renumbering following 5-aa deletion) in the LR act as a mechanical hinge to allow RBD and ED to move relative to one another. This mechanical hinge, which immediately follows the β-turn (residues 74 to 77), is maintained in the

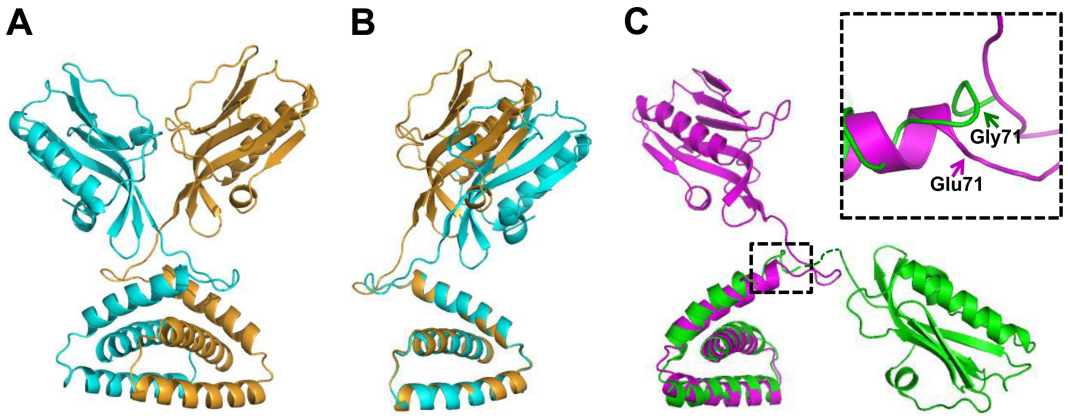


**FIG 4** Structure of H6N6-NS1Δ80-84 and its comparison to the VN/04 H5N1-NS1 structure showing the effect of E71G mutation. (A) The crystal structure of the H6N6-NS1Δ80-84 contains two molecules of NS1 in the asymmetric unit (one colored cyan and the other colored bright orange), which form a closed dimer. (B) Superposition of the two H6N6-NS1Δ80-84 NS1 molecules in the asymmetric unit indicates differences in their ED orientations with respect to RBD. (C) Comparison of the H6N6-NS1Δ80-84 monomer (magenta) and VN/04 H5N1-NS1 monomer (green) (PDB ID 3F5T) by superposition of their RBDs shows the structural changes between the two located at residue 71 (inset) at the end of RBD. In the inset, Gly71 in the VN/04 H5N1-NS1 and Glu71 in the H6N6-NS1Δ80-84 are denoted by green and magenta arrows, respectively.

H6N6 NS1Δ80-84 structure despite the 5-aa deletion and facilitates reorientation of the LR to allow the formation of a closed dimer. It is plausible that one of these hinge residues, since they would be separated by five residues in the context of wild-type H6N6-NS1, can serve the same purpose in the wild-type NS1, allowing further alterations in the angular disposition of the two domains. Since these two residues (Met79 and Pro80) are highly conserved in all the H5N1 NS1s that have a 5-aa deletion, this region may be an important factor in conferring additional structural plasticity to the LR in these NS1s.

**H6N6-NS1Δ80-84 represents the majority of H5N1 NS1s.** To determine why the 5-aa deletion in the H6N6-NS1 did not recapitulate the structural features of the VN/04 H5N1-NS1, we examined all of the available H5N1-NS1 sequences and found that VN/04 H5N1-NS1 has a unique substitution at position 71. In the majority of H5N1-NS1 sequences, the amino acid residue at position 71 is a Glu residue (E71) (Fig. 5). However, a small portion of H5N1-NS1s, including VN/04 H5N1-NS1, contain a Gly residue at position 71. Even in the majority of non-H5N1 NS1s, including the H6N6-NS1 used in our studies, residue 71 is a Glu

```
                50         60         70         80   85      90
AF084285:       LGLDIRTATR EGKHIVERIL EEESDEALKM TIASVPAPRYL TEMTLEEMSR
                50         60         70              80      86
FJ573472:       LGLDIETATR AGKQIVERIL EEESDEALKM -----PASRYL TDMTLEEMSR
EF587281:       LGLDIETATR AGKQIVERIL EEESDEALKM -----PASRYL TDMTLEEMSR
JN588878:       LGLDIETATC AGKQIVERIL EEESDKALKM -----PVSRYL TDMTLEEMSR
JN588879:       LGLDIETATC AGKQIVERIL EKESDKALKM -----PVSRYL TDMTLEEMSR
CY098618:       LGLDIETATR AGKQIVERIL EEESDEALKM -----PTSRYL TDMTLEEMSR
CY098754:       LGLDIETATR AGKQIVERIL EEESDEALKM -----SASRYL TDMTLEEMSR
CY019388:       LGLDIETATR AGKQIVERIL EEESDEALKK -----PASRYL TDMSLEEMSR
CY014259:       LGLDIETSTR AGKQIVERIL EEESDEALKM -----PASRYL IDMTLEEMSR
CY014424:       LGLDIETATR AGKQIVERVL EEESDEALKM -----PASRYL TDMTLEEMSR
AY627894:       LGLDIETATR AGKQIVERIL EEESDKALKM -----PASRYL TDMTLEEMSR
AY818147:       LGLDIETATR AGKQIVERIL EGESDKALKM -----PASRYL TDMTLEEMSR
EF541457:       LGLDIETATR AGKQIVERIL EGESDKALKM -----PAPRYL TDMTLEEMSR
AY526747:       LGLDIETATR AGKQIVERIL EEESDKALKM -----PASRYL TDMTLEEMSR
HM114533:       LGLDIETATR AGKQIVERIL EEESDKALKM -----PASRYL TDMTLKEMSR
CY098733:       LGLDIETATR AGKQIVERIL KEESDEALKM -----PTSRYL TDMTLEEMSR
CY014388:       LGLDIETATR AGKQIVERIL EEESDEALKK -----PASRYL TDMTLEEMSR
CY017642:       LGLDIETATR AGKQIVERIL EEESDEALKK -----PASRYL TDMSLEEMSR
EU499373:       LGLDIETATR AGKQIVERIL EEESDEALKM -----PTSRYL TDMTLEEMSR
CY098612:       LGLDIETATR AGKQIVERIL EEESDEALKM -----PTSRYL TDMTLEEMSR
```

**FIG 5** Representative NS1 sequence alignments from H5N1 influenza viruses obtained from infected individuals. Shown are 20 representative sequences of H5N1 NS1 encoded in influenza viruses obtained from infected individuals. The accession ID number is shown at the far left side of each sequence. The first sequence (AF084285) belongs to an H5N1 NS1 that does not contain the 5-aa residue deletion at the LR. Note that this is a Hong Kong strain isolated in 1997 (residues 50 to 99 are numbered above and shown in black). The remaining 19 sequences depict how the NS1 sequence from influenza A virus strains isolated after 2000 contain an NS1 with residues 80 to 84 deleted at the linker region (because of this deletion, the remaining sequence has been renumbered and is shown above the sequences). Residue 71 is highlighted by a rectangular box to emphasize the consensus E71 found in most H5N1 NS1s. The boldface NS1 sequences that contain a glycine at position 71 (AY818147 and EF511457) belong to the A/VietNam/1203/2004(H5N1) and A/VietNam/1204/2004(H5N1) influenza viruses, respectively. The search criteria used in the Influenza Research Database (51) included a search for protein NS1 of virus type A, human hosts, all geographic groupings, and H5N1 subtype, with removal of duplicate sequences, and no date restrictions were placed on the search.

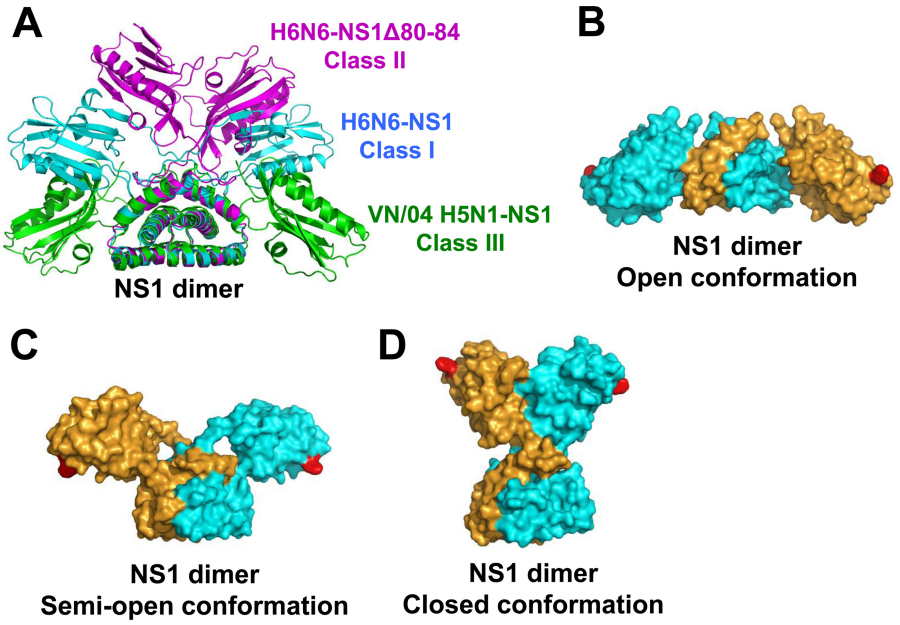


**FIG 6** Structural polymorphism of NS1. (A) Structural superposition of the dimers of H6N6-NS1 (cyan), H6N6-NS1Δ80-84 (magenta), and VN/04 H5N1-NS1 (green) (PDB ID 3F5T) showing the different ED orientations for each NS1. (B) Surface representation of the VN/04 H5N1-NS1 dimer (PDB ID 3F5T) with each NS1 subunit colored in gold and cyan, showing the EDs of flanking the RBD in an "open" conformation, representative of a minority of H5N1 NS1s with the 5-aa deletion and E71G mutation. (C) Surface representation of the H6N6-NS1 dimer (each NS1 subunit is colored as in panel B) showing the EDs at an angular disposition in a "semi-open" conformation representative of the majority of non-H5N1 NS1s. (D) Surface representation of the H6N6-NS1Δ80-84 showing ED participating in intradimeric interactions together with RBD (each NS1 subunit is colored as in panel B) to adopt a "closed" conformation representative of the majority of H5N1 NS1s. Trp187 (shown in red in panels B, C, and D) implicated in type A interdimeric ED-ED interaction is accessible in all three conformational "states."

(data not shown). Thus, it is plausible that H6N6-NS1Δ80-84 is not able to mimic the structural features of VN/04 H5N1 NS1 because of the absence of this E71G mutation, despite having the 5-aa deletion. Comparison of the H6N6-NS1Δ80-84 and VN/04 H5N1-NS1 structures show that the substitution of conformationally flexible Gly at position 71 introduces a local conformational change (Fig. 4C), allowing the LR in VN/04 H5N1-NS1 to chart a different course, resulting in a significant change in the interdomain orientation. The conformational angles of Gly (phi/psi, 3.3°/−130°) in VN/04 H5N1-NS1 are inaccessible for Glu (phi/psi, −93°/9° and −77°/58° for the two molecules in AU). Another important difference in the LR between the two structures is that the region encompassing residues 75 to 79, which contains the β-turn and one of the hinge residues in the H6N6-NS1Δ80-84 structure, is disordered in the VN/04 H5N1-NS1 structure, indicating increased conformational flexibility in this region of the VN/04 H5N1-NS1 structure. With a Glu at position 71 and the 5-aa deletion, which are the common characteristics of the majority of H5N1 NS1s, the structure of H6N6-NS1Δ80-84 can be considered to represent the NS1s of these H5N1 strains.

## DISCUSSION

The crystal structures of the FL H6N6-NS1 and H6N6-NS1Δ80-84 described here, together with previously determined FL VN/04 H5N1-NS1 structure (23), clearly demonstrate that despite any sequence changes, the tertiary structures of the RBD and ED are well conserved. These structures further illustrate that while the RBD-RBD dimer remains invariant, the ED can engage in multiple types of intermolecular interactions (with a PISA value of ~0.3) to promote multimerization of NS1. This observation is consistent with the notion that while the RBD provides the necessary module for the formation of the NS1 dimer and for initiating the interactions with dsRNA, the ED facilitates further encapsidation of the dsRNA through cooperative formation of higher-order oligomers (32). The requirement of the ED for dsRNA interaction has been experimentally demonstrated, and one of the ED-ED interactions that has been deemed necessary for cooperative binding to dsRNA is the type A ED-ED interactions involving W187 (32, 33). Such a type of interaction is clearly observed in both H6N6-NS1 and VN/04 H5N1-NS1 structures. It should be noted that even in the H6N6-NS1Δ80-84 structure, although the ED is involved intradimeric interactions to form a closed dimer, W187 is surface exposed and can associate to form chain-like structures through type A ED-ED interactions to cooperatively interact with dsRNA. However, our mutational studies of the H6N6-NS1 W187Y show that the type A ED-ED interaction is not obligatory for the formation of dimers or the higher-order oligomers. Hence, the non-A-type ED-ED interactions may be at play in the context of other functions of NS1 during the virus infection.

The conservation of the RBD-RBD dimer in all of these structures, together with the formation of the NS1 dimer through intertwined LR interactions, as observed in our FL H6N6-NS1, strongly suggests that NS1 has an intrinsic propensity to form dimers. However, the structure of the ED in complex with p85β subunit of PI3K (13) indicates the possibility of NS1 existing in a monomeric state. One possibility is that interaction with p85β subunit destabilizes the RBD dimer; alternatively, this interaction just alters interdomain orientation to bind ED without disrupting the RBD dimer. The structure of NS1-ED in complex with the F2F3 fragment of CPSF30 has also been determined (14). In this

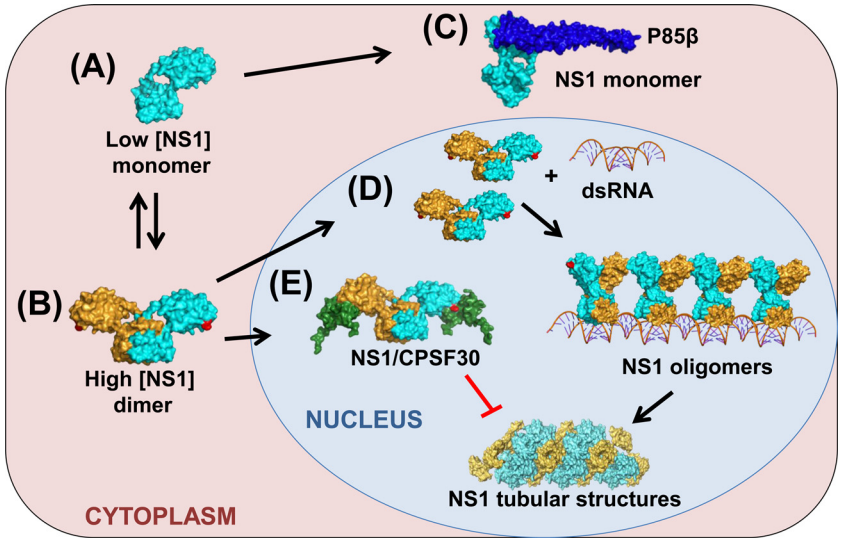


**FIG 7** Proposed model of NS1 oligomeric states during infection. (A) Early in infection, NS1 monomers (cyan) are present in the cell due to the low concentration of NS1. (B) NS1 monomers likely exist in equilibrium with dimeric forms of NS1 (each NS1 monomer shown in cyan and gold). (C) Monomeric NS1 (cyan) may be found when it forms a complex with the P85β subunit (blue; we used PDB ID 3L4Q superimposed onto the H6N6-NS1 structure) of PI3K (13) and would be localized to the plasma membrane. (D) NS1 dimers (each NS1 monomer is shown in cyan and gold; Trp187 is shown in red) localized in the nucleus, upon binding to dsRNA and via the exposed Trp187 (shown in red), can help in the recruitment of other NS1 dimers to cooperatively bind to dsRNA. Once NS1 dimers cover the entirety of the dsRNA species, these will resemble tubular structures that encase dsRNA, as has been proposed previously (23, 32). (E) FL NS1 dimer (the dimer is colored as in panel B) in complex with CPSF30 shown in green (conceptual model based on the ED structure in complex with F2F3 fragment of CPSF30 [PDB ID: 2RHK]) that can be found in the nucleus and may inhibit the formation of oligomers by NS1 due to the fact that NS1's ability to oligomerize when binding to dsRNA requires Trp187, which is occluded when CPSF30 interacts with NS1. The binding affinity of NS1 for each of the ligands such as RNA or CPSF30 is likely modulated in a strain-dependent manner not only by the preferred conformational state and structural plasticity around this state for each strain but also by subtle sequence changes in the ligand binding interfaces.

structure, the ED as a head-to-head dimer binds to two molecules of the F2F3 fragment of CPSF30, forming a heterotetrameric complex. This type of ED-ED dimer is not observed in any of the FL NS1 structures. Although these studies point to context-dependent ED-ED interactions, further structural studies of FL NS1 in complex with these host proteins are required to fully understand their interactions with NS1.

Our structural studies in conjunction with the VN/04 H5N1-NS1 provide representative structures defining three broad classes of NS1 (Fig. 6A). Class I, represented by our H6N6-NS1, consists of NS1s that contain a longer linker and the consensus Glu at position 71, which exemplifies the majority of NS1s. Class II, represented by our H6N6-NS1Δ80-84, consists of those NS1s that contain the 5-aa deletion and the consensus Glu at position 71, which would represent most H5N1 NS1s. Class III, represented by the VN/04 H5N1-NS1 structure, would encompass a minor class of H5N1 NS1s that contain the five residue deletion and the E71G substitution.

These structures of the FL-NS1 also provide an exquisite structural sampling of various conformational states of NS1 (Fig. 6A) that based on the orientation of the ED can be summarized as "open" (VN/04 H5N1-NS1) (Fig. 6B), "semi-open" (H6N6-NS1) (Fig. 6C), and "closed" (H6N6-NS1Δ80-84) (Fig. 6D) conformations. Although the preference for these states is clearly dictated by determinants such as linker length, residue composition at position 71, and a mechanical hinge, it is also possible that any particular NS1, because of the flexibility that appears to be inherent in the LR, could sample the conformational space around these states to engage ED in different quaternary interactions. This in turn would permit NS1 to participate in specific protein-protein or RNA-protein interactions that allow for the known multifunctionality of NS1 (7). Such conformational plasticity could provide a mechanism for auto-regulating NS1 functions, depending on its temporal distribution, posttranslational modifications (phosphorylation [36, 37] and sumoylation [38, 39]), and nuclear or cellular localization, during the course of virus infection.

A simple working model that can be proposed based on the available information is depicted in Fig. 7. Early in infection, when the concentration of NS1 is low, NS1 may exist as a monomer (Fig. 7A) or at a thermodynamic equilibrium between monomer and dimeric forms (Fig. 7B). Monomeric NS1 may be favored when NS1 undergoes structural changes, for instance, when in complex to PI3K (13) (Fig. 7C). Later in infection, as the concentration of NS1 increases, dimeric forms of NS1 may be the predominant species and may come together to bind dsRNA, forming oligomeric/tubular structures, as has been proposed previously via the type A ED-ED interactions (23, 32) (Fig. 7D). The formation of these oligomeric structures via the type A ED-ED involves Trp187, the same residue that is in close proximity to the binding site of CPSF30. Thus, the formation of oligomers by NS1 may be inhibited in the case where NS1 is bound to CPSF30 (Fig. 7E) (14), although the precise orientation of the ED required to bind CPSF30, in the context of the FL NS1, is unclear. In addition to these interactions, NS1 also interacts with several other host proteins, including TRIM25 (40), PKR (41), and Scribble (42, 43). Several studies have shown that these interactions are modulated in a strain-specific fashion (2, 18, 42, 44–48), including the NS1s of H5N1 strains, which show weak binding to CPSF30 (2, 14, 49) and cytokine resistance (1, 50), in contrast to the NS1s of non-H5N1 strains. We surmise that the observed structural polymor-

phism of NS1 across the strains and the structural plasticity that is allowed within any NS1 may be the basis for strain-dependent modulation of these interactions.

## ACKNOWLEDGMENTS

This study was supported by National Institutes of Health grant R21 AI083396 (A.P.R.) and Robert Welch grant Q1279 (B.V.V.P.).

We acknowledge the use of the synchrotron beamline at Advanced Light Source (5.0.1), Berkeley, CA, for diffraction data collection.

## REFERENCES

1. **Seo SH, Hoffmann E, Webster RG.** 2002. Lethal H5N1 influenza viruses escape host antiviral cytokine responses. Nat. Med. **8:**950–954. http://dx.doi.org/10.1038/nm757.
2. **Twu KY, Kuo RL, Marklund J, Krug RM.** 2007. The H5N1 influenza virus NS genes selected after 1998 enhance virus replication in mammalian cells. J. Virol. **81:**8112–8121. http://dx.doi.org/10.1128/JVI.00006-07.
3. **Ma W, Brenner D, Wang Z, Dauber B, Ehrhardt C, Hogner K, Herold S, Ludwig S, Wolff T, Yu K, Richt JA, Planz O, Pleschka S.** 2010. The NS segment of an H5N1 highly pathogenic avian influenza virus (HPAIV) is sufficient to alter replication efficiency, cell tropism, and host range of an H7N1 HPAIV. J. Virol. **84:**2122–2133. http://dx.doi.org/10.1128/JVI.01668-09.
4. **Egorov A, Brandt S, Sereinig S, Romanova J, Ferko B, Katinger D, Grassauer A, Alexandrova G, Katinger H, Muster T.** 1998. Transfectant influenza A viruses with long deletions in the NS1 protein grow efficiently in Vero cells. J. Virol. **72:**6437–6441.
5. **Garcia-Sastre A, Egorov A, Matassov D, Brandt S, Levy DE, Durbin JE, Palese P, Muster T.** 1998. Influenza A virus lacking the NS1 gene replicates in interferon-deficient systems. Virology **252:**324–330. http://dx.doi.org/10.1006/viro.1998.9508.
6. **Kochs G, Koerner I, Thiel L, Kothlow S, Kaspers B, Ruggli N, Summerfield A, Pavlovic J, Stech J, Staeheli P.** 2007. Properties of H7N7 influenza A virus strain SC35M lacking interferon antagonist NS1 in mice and chickens. J. Gen. Virol. **88:**1403–1409. http://dx.doi.org/10.1099/vir.0.82764-0.
7. **Hale BG, Randall RE, Ortin J, Jackson D.** 2008. The multifunctional NS1 protein of influenza A viruses. J. Gen. Virol. **89:**2359–2376. http://dx.doi.org/10.1099/vir.0.2008/004606-0.
8. **Min JY, Krug RM.** 2006. The primary function of RNA binding by the influenza A virus NS1 protein in infected cells: inhibiting the 2′-5′ oligo(A) synthetase/RNase L pathway. Proc. Natl. Acad. Sci. U. S. A. **103:**7100–7105. http://dx.doi.org/10.1073/pnas.0602184103.
9. **Cheng A, Wong SM, Yuan YA.** 2009. Structural basis for dsRNA recognition by NS1 protein of influenza A virus. Cell Res. **19:**187–195. http://dx.doi.org/10.1038/cr.2008.288.
10. **Liu J, Lynch PA, Chien CY, Montelione GT, Krug RM, Berman HM.** 1997. Crystal structure of the unique RNA-binding domain of the influenza virus NS1 protein. Nat. Struct. Biol. **4:**896–899. http://dx.doi.org/10.1038/nsb1197-896.
11. **Bornholdt ZA, Prasad BV.** 2006. X-ray structure of influenza virus NS1 effector domain. Nat. Struct. Mol. Biol. **13:**559–560. http://dx.doi.org/10.1038/nsmb1099.
12. **Kerry PS, Long E, Taylor MA, Russell RJ.** 2011. Conservation of a crystallographic interface suggests a role for beta-sheet augmentation in influenza virus NS1 multifunctionality. Acta Crystallogr. Sect. F Struct. Biol. Chryst. Commun. **67:**858–861. http://dx.doi.org/10.1107/S1744309111019312.
13. **Hale BG, Kerry PS, Jackson D, Precious BL, Gray A, Killip MJ, Randall RE, Russell RJ.** 2010. Structural insights into phosphoinositide 3-kinase activation by the influenza A virus NS1 protein. Proc. Natl. Acad. Sci. U. S. A. **107:**1954–1959. http://dx.doi.org/10.1073/pnas.0910715107.
14. **Das K, Ma LC, Xiao R, Radvansky B, Aramini J, Zhao L, Marklund J, Kuo RL, Twu KY, Arnold E, Krug RM, Montelione GT.** 2008. Structural basis for suppression of a host antiviral response by influenza A virus. Proc. Natl. Acad. Sci. U. S. A. **105:**13093–13098. http://dx.doi.org/10.1073/pnas.0805213105.
15. **Kerry PS, Ayllon J, Taylor MA, Hass C, Lewis A, Garcia-Sastre A, Randall RE, Hale BG, Russell RJ.** 2011. A transient homotypic interaction model for the influenza A virus NS1 protein effector domain. PLoS One **6:**e17946. http://dx.doi.org/10.1371/journal.pone.0017946.
16. **Xia S, Robertus JD.** 2010. X-ray structures of NS1 effector domain mutants. Arch. Biochem. Biophys. **494:**198–204. http://dx.doi.org/10.1016/j.abb.2009.12.008.
17. **Hale BG, Barclay WS, Randall RE, Russell RJ.** 2008. Structure of an avian influenza A virus NS1 protein effector domain. Virology **378:**1–5. http://dx.doi.org/10.1016/j.virol.2008.05.026.
18. **Hayman A, Comely S, Lackenby A, Murphy S, McCauley J, Goodbourn S, Barclay W.** 2006. Variation in the ability of human influenza A viruses to induce and inhibit the IFN-beta pathway. Virology **347:**52–64. http://dx.doi.org/10.1016/j.virol.2005.11.024.
19. **Suarez DL, Perdue ML.** 1998. Multiple alignment comparison of the nonstructural genes of influenza A viruses. Virus Res. **54:**59–69. http://dx.doi.org/10.1016/S0168-1702(98)00011-2.
20. **Dundon WG, Capua I.** 2009. A closer look at the NS1 of influenza virus. Viruses **1:**1057–1072. http://dx.doi.org/10.3390/v1031057.
21. **Zhan L, Rosenberg A, Bergami KC, Yu M, Xuan Z, Jaffe AB, Allred C, Muthuswamy SK.** 2008. Deregulation of scribble promotes mammary tumorigenesis and reveals a role for cell polarity in carcinoma. Cell **135:**865–878. http://dx.doi.org/10.1016/j.cell.2008.09.045.
22. **Long JX, Peng DX, Liu YL, Wu YT, Liu XF.** 2008. Virulence of H5N1 avian influenza virus enhanced by a 15-nucleotide deletion in the viral nonstructural gene. Virus Genes **36:**471–478. http://dx.doi.org/10.1007/s11262-007-0187-8.
23. **Bornholdt ZA, Prasad BV.** 2008. X-ray structure of NS1 from a highly pathogenic H5N1 influenza virus. Nature **456:**985–988. http://dx.doi.org/10.1038/nature07444.
24. **Battye TG, Kontogiannis L, Johnson O, Powell HR, Leslie AG.** 2011. iMOSFLM: a new graphical interface for diffraction-image processing with MOSFLM. Acta Crystallogr. D Biol. Crystallogr. **67:**271–281. http://dx.doi.org/10.1107/S0907444910048675.
25. **Winn MD, Ballard CC, Cowtan KD, Dodson EJ, Emsley P, Evans PR, Keegan RM, Krissinel EB, Leslie AG, McCoy A, McNicholas SJ, Murshudov GN, Pannu NS, Potterton EA, Powell HR, Read RJ, Vagin A, Wilson KS.** 2011. Overview of the CCP4 suite and current developments. Acta Crystallogr. D Biol. Crystallogr. **67:**235–242. http://dx.doi.org/10.1107/S0907444910045749.
26. **Strong M, Sawaya MR, Wang S, Phillips M, Cascio D, Eisenberg D.** 2006. Toward the structural genomics of complexes: crystal structure of a PE/PPE protein complex from *Mycobacterium tuberculosis*. Proc. Natl. Acad. Sci. U. S. A. **103:**8060–8065. http://dx.doi.org/10.1073/pnas.0602606103.
27. **Adams PD, Afonine PV, Bunkoczi G, Chen VB, Davis IW, Echols N, Headd JJ, Hung LW, Kapral GJ, Grosse-Kunstleve RW, McCoy AJ, Moriarty NW, Oeffner R, Read RJ, Richardson DC, Richardson JS, Terwilliger TC, Zwart PH.** 2010. PHENIX: a comprehensive Python-based system for macromolecular structure solution. Acta Crystallogr. D Biol. Crystallogr. **66:**213–221. http://dx.doi.org/10.1107/S0907444909052925.
28. **Brunger AT.** 1992. Free R value: a novel statistical quantity for assessing the accuracy of crystal structures. Nature **355:**472–475. http://dx.doi.org/10.1038/355472a0.
29. **Emsley P, Cowtan K.** 2004. Coot: model-building tools for molecular graphics. Acta Crystallogr. D Biol. Crystallogr. **60:**2126–2132. http://dx.doi.org/10.1107/S0907444904019158.
30. **Skubak P, Pannu NS.** 2011. Reduction of density-modification bias by beta correction. Acta Crystallogr. D Biol. Crystallogr. **67:**345–354. http://dx.doi.org/10.1107/S0907444911002083.
31. **Davis IW, Leaver-Fay A, Chen VB, Block JN, Kapral GJ, Wang X, Murray LW, Arendall WB, III, Snoeyink J, Richardson JS, Richardson DC.** 2007. MolProbity: all-atom contacts and structure validation for proteins and nucleic acids. Nucleic Acids Res. **35:**W375–W383. http://dx.doi.org/10.1093/nar/gkm216.
32. **Aramini JM, Ma LC, Zhou L, Schauder CM, Hamilton K, Amer BR, Mack TR, Lee HW, Ciccosanti CT, Zhao L, Xiao R, Krug RM, Montelione GT.** 2011. Dimer interface of the effector domain of nonstructural protein 1 from influenza A virus: an interface with multiple functions. J. Biol. Chem. **286:**26050–26060. http://dx.doi.org/10.1074/jbc.M111.248765.
33. **Ayllon J, Russell RJ, Garcia-Sastre A, Hale BG.** 2012. Contribution of NS1 effector domain dimerization to influenza A virus replication and virulence. J. Virol. **86:**13095–13098. http://dx.doi.org/10.1128/JVI.02237-12.
34. **Xia S, Monzingo AF, Robertus JD.** 2009. Structure of NS1A effector domain from the influenza A/Udorn/72 virus. Acta Crystallogr. D Biol. Crystallogr. **65:**11–17. http://dx.doi.org/10.1107/S0907444908032186.

35. **Hayward S, Berendsen HJ.** 1998. Systematic analysis of domain motions in proteins from conformational change: new results on citrate synthase and T4 lysozyme. Proteins **30:**144–154. http://dx.doi.org/10.1002/(SICI)1097-0134(19980201)30:2<144::AID-PROT4>3.3.CO;2-I.
36. **Hale BG, Knebel A, Botting CH, Galloway CS, Precious BL, Jackson D, Elliott RM, Randall RE.** 2009. CDK/ERK-mediated phosphorylation of the human influenza A virus NS1 protein at threonine-215. Virology **383:**6–11. http://dx.doi.org/10.1016/j.virol.2008.10.002.
37. **Hsiang TY, Zhou L, Krug RM.** 2012. Roles of the phosphorylation of specific serines and threonines in the NS1 protein of human influenza A viruses. J. Virol. **86:**10370–10376. http://dx.doi.org/10.1128/JVI.00732-12.
38. **Santos A, Pal S, Chacon J, Meraz K, Gonzalez J, Prieto K, Rosas-Acosta G.** 2013. SUMOylation affects the interferon blocking activity of the influenza A nonstructural protein NS1 without affecting its stability or cellular localization. J. Virol. **87:**5602–5620. http://dx.doi.org/10.1128/JVI.02063-12.
39. **Xu K, Klenk C, Liu B, Keiner B, Cheng J, Zheng BJ, Li L, Han Q, Wang C, Li T, Chen Z, Shu Y, Liu J, Klenk HD, Sun B.** 2011. Modification of nonstructural protein 1 of influenza A virus by SUMO1. J. Virol. **85:**1086–1098. http://dx.doi.org/10.1128/JVI.00877-10.
40. **Gack MU, Albrecht RA, Urano T, Inn KS, Huang IC, Carnero E, Farzan M, Inoue S, Jung JU, Garcia-Sastre A.** 2009. Influenza A virus NS1 targets the ubiquitin ligase TRIM25 to evade recognition by the host viral RNA sensor RIG-I. Cell Host Microbe **5:**439–449. http://dx.doi.org/10.1016/j.chom.2009.04.006.
41. **Hatada E, Saito S, Fukuda R.** 1999. Mutant influenza viruses with a defective NS1 protein cannot block the activation of PKR in infected cells. J. Virol. **73:**2425–2433.
42. **Liu H, Golebiewski L, Dow EC, Krug RM, Javier RT, Rice AP.** 2010. The ESEV PDZ-binding motif of the avian influenza A virus NS1 protein protects infected cells from apoptosis by directly targeting Scribble. J. Virol. **84:**11164–11174. http://dx.doi.org/10.1128/JVI.01278-10.
43. **Golebiewski L, Liu H, Javier RT, Rice AP.** 2011. The avian influenza virus NS1 ESEV PDZ binding motif associates with Dlg1 and Scribble to disrupt cellular tight junctions. J. Virol. **85:**10639–10648. http://dx.doi.org/10.1128/JVI.05070-11.
44. **Kochs G, Garcia-Sastre A, Martinez-Sobrido L.** 2007. Multiple anti-interferon actions of the influenza A virus NS1 protein. J. Virol. **81:**7011–7021. http://dx.doi.org/10.1128/JVI.02581-06.
45. **Melen K, Kinnunen L, Fagerlund R, Ikonen N, Twu KY, Krug RM, Julkunen I.** 2007. Nuclear and nucleolar targeting of influenza A virus NS1 protein: striking differences between different virus subtypes. J. Virol. **81:**5995–6006. http://dx.doi.org/10.1128/JVI.01714-06.
46. **Hale BG, Steel J, Medina RA, Manicassamy B, Ye J, Hickman D, Hai R, Schmolke M, Lowen AC, Perez DR, Garcia-Sastre A.** 2010. Inefficient control of host gene expression by the 2009 pandemic H1N1 influenza A virus NS1 protein. J. Virol. **84:**6909–6922. http://dx.doi.org/10.1128/JVI.00081-10.
47. **Kuo RL, Zhao C, Malur M, Krug RM.** 2010. Influenza A virus strains that circulate in humans differ in the ability of their NS1 proteins to block the activation of IRF3 and interferon-beta transcription. Virology **408:**146–158. http://dx.doi.org/10.1016/j.virol.2010.09.012.
48. **Ayllon J, Hale BG, Garcia-Sastre A.** 2012. Strain-specific contribution of NS1-activated phosphoinositide 3-kinase signaling to influenza A virus replication and virulence. J. Virol. **86:**5366–5370. http://dx.doi.org/10.1128/JVI.06722-11.
49. **Kuo RL, Krug RM.** 2009. Influenza a virus polymerase is an integral component of the CPSF30-NS1A protein complex in infected cells. J. Virol. **83:**1611–1616. http://dx.doi.org/10.1128/JVI.01491-08.
50. **Seo SH, Hoffmann E, Webster RG.** 2004. The NS1 gene of H5N1 influenza viruses circumvents the host antiviral cytokine responses. Virus Res. **103:**107–113. http://dx.doi.org/10.1016/j.virusres.2004.02.022.
51. **Squires RB, Noronha J, Hunt V, Garcia-Sastre A, Macken C, Baumgarth N, Suarez D, Pickett BE, Zhang Y, Larsen CN, Ramsey A, Zhou L, Zaremba S, Kumar S, Deitrich J, Klem E, Scheuermann RH.** 2012. Influenza research database: an integrated bioinformatics resource for influenza research and surveillance. Influenza Other Respir. Viruses **6:**404–416. http://dx.doi.org/10.1111/j.1750-2659.2011.00331.x.